Investigation of the diocotron instability of an infinitely wide sheet electron beam by using the macroscopic cold-fluid model theory*

Han Ying(韩 莹)[a)b)†] and Ruan Cun-Jun(阮存军)[a)]

[a)] *Key Laboratory of High Power Microwave Sources and Technologies, Institute of Electronics, Chinese Academy of Sciences, Beijing* 100190, *China*

[b)] *Graduate University of the Chinese Academy of Sciences, Beijing* 100049, *China*

(Received 22 November 2010; revised manuscript received 28 April 2011)

This paper investigates the diocotron instability of an infinitely wide relativistic sheet electron beam in conducting walls propagating through a uniform magnetic field by using the macroscopic cold-fluid model theory. Assuming low-frequency perturbations with long axial wavelengths, the eigenvalue equation and the dispersion relation are acquired for a sheet electron beam with sharp boundary profile and uniform density. The results presented in this paper has developed the use of the macroscopic cold-fluid model theory by extending the parameter of the electron cyclotron frequency $\omega_{\rm c}$ to a wider usage range, which is restricted to be much larger than the plasma frequency $\omega_{\rm p}$ in the previous research work. Theoretical analyses and numerical calculations indicate that the transport of the sheet electron beam will be completely stabilized by augmenting the normalized beam thickness to a conductor gap larger than a threshold $\lambda_{\rm b}$, which is greatly dependent on the parameter $\omega_{\rm c}/\omega_{\rm p}$. The larger $\omega_{\rm c}/\omega_{\rm p}$ is, the smaller $\lambda_{\rm b}$ will be needed. Moreover, the system parameters, including the wave number k_x of the perturbations and the relativistic mass factor $\gamma_{\rm b}$, will also influence the growth rate of diocotron instability obviously.

Keywords: diocotron instability, macroscopic cold-fluid model, sheet electron beam

PACS: 41.75.–i, 41.85.–p, 41.85.Ja, 41.90.+e **DOI:** 10.1088/1674-1056/20/10/104101

1. Introduction

Sheet electron beams have recently become very attractive for numerous applications varying from high power microwave sources to an advanced accelerator. The sheet beam has a large aspect ratio so that it provides a higher total current but a lower current density. Space charge effects are considerably decreased, which makes a sheet beam more suitable for high frequency and high power applications.

The key challenges in realizing sheet beam devices are the focusing and stable transport of a sheet beam. It is well known that a sheet beam unstably propagates through a uniform magnetic field due to $\boldsymbol{E} \times \boldsymbol{B}$ velocity shear effects. This diocotron instability will result in beam kinks, vortices and eventual filament. This was experimentally demonstrated as early as in the 1950s.[1−3] Subsequently, theoretical studies of diocotron instability have continued to develop.[4−7] In Chen's article[8] the diocotron instability of a relativistic annular electron beam in a conducting tube was investigated in the parameter region where the plasma frequency approached the cyclotron frequency. Also the diocotron instability of a relativistic sheet electron beam in a rectangular conducting tube was investigated by Uhm[9] for the case of a partially neutralized beam propagating through a strong magnetic field. For the purpose of avoiding instability, periodic focusing fields, including periodic cusped magnetic fields and wiggler magnetic fields, were proposed according to the classical works by Booske *et al.*[10,11] Periodic focusing fields became the focus of theoretical studies from then on and have been carried out successfully in practical applications. A W-band sheet beam klystron with periodic cusped magnetic fields has been built and tested at the Stanford Linear Accelerator Centre.[12] The beam transmission was over 90% with a 74-kV, 3.6-A elliptical cross-section sheet electron beam. However, the periodic magnetic configuration is more complex and prone to magnetic field errors due to mechanical misalignments, which increases the difficulty of manufacture. Compared

*Project supported by the National Natural Science Foundation of China (Grant Nos. 60501019, 10775139, and 60971073).

†Corresponding author. E-mail: helen_han@139.com

© 2011 Chinese Physical Society and IOP Publishing Ltd

with the periodic magnetic fields, we find that the advantage of a solenoid focusing configuration is substantial. It has a simpler configuration, lower cost and an achievable higher field. Therefore, we choose a solenoid structure to accomplish the focusing and stable transport of an elliptical sheet beam in our design of a W-band sheet beam klystron. The sample tube has been built and tested successfully.[13,14] The transmission is up to over 95% at voltages from 35 kV to 80 kV.

It is obvious that we need to examine the diocotron instability of a sheet electron beam propagating through a solenoid magnetic field in order to guide practical design. The elliptical sheet beam and drift tube can be considered as semi-infinite structures because one transverse dimension is much larger than the other dimension. This paper studies the diocotron instability of an infinitely wide relativistic sheet electron beam in grounded conducting walls propagating through a uniform magnetic field. In particular, considering more current carried by a sheet beam, we find that the uniform magnetic field may have more difficulty to keep up with the current. The investigation in the subsequent analysis extends the parameter region of electron cyclotron frequency $\omega_{\rm c}$ varying from having the order of plasma frequency $\omega_{\rm p}$ to much larger than that from previous works, in which $\omega_{\rm c}$ is merely much larger than $\omega_{\rm p}$. The basic equilibrium theory is reviewed in Section 2 by making use of a macroscopic cold-fluid model. In Section 3 we derive the general eigenvalue equation [Eq. (27)] and the dispersion relation [Eqs. (32) and (33)] of the diocotron instability for low-frequency perturbations with long axial wavelengths, abandoning the restrictive condition $\omega_{\rm c} \gg \omega_{\rm p}$. In succession, the diocotron instability of a semi-infinite sheet beam with a sharp boundary and uniform density profile [Eq. (13)] is investigated by utilizing the dispersion relation for a broad range of system parameters including the ratio h/b (where h is the beam thickness, b is the gap of conducting walls), the wave number k_x of the perturbations in the x direction, and the relativistic mass factor $\gamma_{\rm b}$.

2. Equilibrium of a semi-infinite sheet electron beam configuration

We consider a sheet electron beam propagating parallel to an axial magnetic field $B_0\boldsymbol{e}_z$ with the velocity of $v_{\rm b}\boldsymbol{e}_z$ in grounded conducting walls, where $\boldsymbol{e}_z$ is a unit vector along the z axis. The sheet beam and the conducting walls both have infinite width along the x axis.

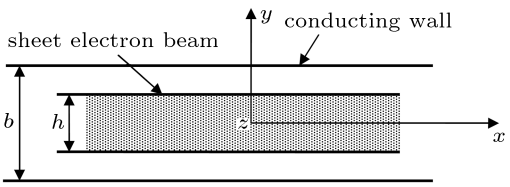


Fig. 1. The semi-infinite sheet electron beam configuration.

The equilibrium analysis is carried out by adopting a macroscopic cold-fluid model, where the electron motion is assumed to be laminar. The equation of motion and the continuity equation for the electron fluid can be expressed as[9]

$$\left(\frac{\partial}{\partial t}+\boldsymbol{v}\cdot\boldsymbol{\nabla}\right)\gamma m\boldsymbol{v}=-e\left(\boldsymbol{E}+\boldsymbol{v}\times\boldsymbol{B}\right), \tag{1}$$

and

$$\frac{\partial n}{\partial t}+\boldsymbol{\nabla}\cdot(n\boldsymbol{v})=0, \tag{2}$$

where $-e$ and m are the electron charge and rest mass, respectively, $\boldsymbol{v}$ and n are the electron velocity and electron density of the electron fluid element, respectively, $\boldsymbol{E}$ and $\boldsymbol{B}$ are the space-charge electric and magnetic fields, respectively, $\gamma=\left(1-\boldsymbol{v}\cdot\boldsymbol{v}/c^2\right)^{-1/2}$ is the relativistic mass factor, c is the velocity of light in vacuum. We assume that the focusing magnetic field is large enough to make the beam laminar. The motion of the beam electrons is predominantly in the z direction, and the axial velocity is large in comparison with the transverse velocity. Then the relativistic mass factor of the beam is specialized to $\gamma_{\rm b}=\left(1-\beta_{\rm b}^2\right)^{-1/2}$, where $\beta_{\rm b}=v_{\rm b}/c$.

It is evident that all the variables are independent of the x and z directions since the beam is long enough. Hence, we express the equilibrium electric and magnetic fields of the semi-infinite sheet beam shown in Fig. 1 as

$$\boldsymbol{E}\left(y\right)=E_{0y}\left(y\right)\boldsymbol{e}_y, \tag{3}$$

and

$$\boldsymbol{B}\left(y\right)=B_{0x}\left(y\right)\boldsymbol{e}_x+B_0\boldsymbol{e}_z, \tag{4}$$

where $\boldsymbol{e}_x$ and $\boldsymbol{e}_y$ are unit vectors along the x and y axes, respectively, E_{0y} is the space-charge electric field in the y direction, B_{0x} is the self-magnetic field in the x direction. The self-electric and self-magnetic fields are determined from the Maxwell equations

$$\frac{{\rm d}^2\phi_0(y)}{{\rm d}y^2}=\frac{en_0(y)}{\varepsilon_0}, \tag{5}$$

and

$$\frac{\mathrm{d}^2 A_{0z}(y)}{\mathrm{d}y^2} = \frac{\beta_\mathrm{b} e n_0(y)}{c\varepsilon_0}, \tag{6}$$

where ϕ_0 and A_{0z} are the equilibrium scalar electric and vector magnetic potentials, respectively. Defining the equilibrium self-electric potential ψ_0 as

$$\psi_0(y) = \phi_0(y) - c\beta_\mathrm{b} A_{0z}(y), \tag{7}$$

we can express Eqs. (5) and (6) as follows:

$$\frac{\mathrm{d}^2 \psi_0(y)}{\mathrm{d}y^2} = \frac{e n_0(y)}{\gamma_\mathrm{b}^2 \varepsilon_0}. \tag{8}$$

The boundary condition of the self-electric potential $\psi_0(y)$ is $\psi_0(\pm b/2) = 0$ by virtue of the grounded conducting walls. According to Eqs. (5), (6), and (7), the equilibrium self-fields in Eqs. (3) and (4) are expressed as

$$E_{0y}(y) = -\frac{\mathrm{d}\phi_0(y)}{\mathrm{d}y} = -\gamma_\mathrm{b}^2 \frac{\mathrm{d}\psi_0(y)}{\mathrm{d}y}, \tag{9}$$

and

$$B_{0x}(y) = \frac{\mathrm{d}A_{0z}(y)}{\mathrm{d}y} = \frac{\beta_\mathrm{b}\gamma_\mathrm{b}^2}{c}\frac{\mathrm{d}\psi_0(y)}{\mathrm{d}y}. \tag{10}$$

In the equilibrium situation, the ponderomotive force acting on the electron fluid element is matched in the y direction. There will be

$$E_{0y}(y) - v_{0x}(y)B_0 + v_\mathrm{b} B_{0x}(y) = 0 \tag{11}$$

from Eq. (1). Here, v_{0x} is the mean velocity along the x direction. Substituting Eqs. (9) and (10) into Eq. (11), we can obtain

$$v_{0x}(y) = -\frac{1}{B_0}\frac{\mathrm{d}\psi_0(y)}{\mathrm{d}y}. \tag{12}$$

For the sharp boundary and uniform density profile given by

$$n_0(y) = \begin{cases} n_\mathrm{b}, & -h/2 < y < h/2, \\ 0, & \text{otherwise}, \end{cases} \tag{13}$$

we integrate Eq. (8) integral and substitute it into Eq. (12). After a simple algebraic manipulation, the mean velocity in the x direction can be derived as

$$v_{0x}(y) = -2\omega_\mathrm{D} y. \tag{14}$$

Here, the diocotron frequency ω_D is defined by

$$\omega_\mathrm{D} = \omega_\mathrm{p}^2/2\gamma_\mathrm{b}^2\omega_\mathrm{c}, \tag{15}$$

where $\omega_\mathrm{p}^2 = e^2 n_\mathrm{b}/\gamma_\mathrm{b} m\varepsilon_0$ is the square of the plasma frequency and $\omega_\mathrm{c} = eB_0/\gamma_\mathrm{b} m$ is the electron cyclotron frequency, ε_0 is the dielectric constant in vacuum.

3. Diocotron instability analysis

3.1. General eigenvalue equation and dispersion relation

In this section, the general eigenvalue equation for fluid perturbations about the equilibrium state described in Section 2 is derived and the dispersion relation is deduced subsequently by theoretical analyses. To make the present solution tractable, we assume the perturbations with long axial wavelengths

$$k_z h/2 \ll 2\pi, \tag{16}$$

where k_z is the axial wave number of the perturbation. The above assumption means that the perturbed electromagnetic fields in the axial direction can be neglected. We also assume that the diocotron instability is characterized by low-frequency perturbations

$$|\omega - k_z\beta_\mathrm{b} c| \ll |k_x c|, \tag{17}$$

which means that the perturbation is basically electrostatic in the beam frame. Therefore, the perturbed fields in the laboratory frame can be derived from the perturbed scalar electric ($\delta\phi$) and vector magnetic (δA_z) potentials, which are determined by

$$\left(\frac{\partial^2}{\partial x^2} + \frac{\partial^2}{\partial y^2}\right)\delta\phi(x,y) = \frac{e}{\varepsilon_0}\delta n(x,y), \tag{18}$$

$$\left(\frac{\partial^2}{\partial x^2} + \frac{\partial^2}{\partial y^2}\right)\delta A_z(x,y) = \frac{\beta_\mathrm{b} e}{c\varepsilon_0}\delta n(x,y), \tag{19}$$

where δn is the perturbed charge density. Defining the perturbed potential

$$\delta\psi(x,y) = \delta\phi(x,y) - c\beta_\mathrm{b}\delta A_z(x,y), \tag{20}$$

we obtain the perturbed electrostatic field ($\delta\boldsymbol{E}$) and magnetostatic field ($\delta\boldsymbol{B}$) as follows:

$$\delta\boldsymbol{E}(x,y) = -\nabla_\perp\delta\phi(x,y) = -\gamma_\mathrm{b}^2\nabla_\perp\delta\psi(x,y), \tag{21}$$

$$\delta\boldsymbol{B}(x,y) = \nabla_\perp \times \delta A_z(x,y) = \frac{\gamma_\mathrm{b}^2\beta_\mathrm{b}}{c}\nabla_\perp \times \delta\psi(x,y), \tag{22}$$

where $\nabla_\perp = \partial/\partial\boldsymbol{x}_\perp$, $\boldsymbol{x}_\perp = x\boldsymbol{e}_x + y\boldsymbol{e}_y$.

All the perturbed quantities are Fourier decomposed according to

$$\delta\Phi(x,y,z,t) = \delta\Phi(y)\exp[\mathrm{i}(k_x x + k_z z - \omega t)], \tag{23}$$

where $\delta\Phi$ represents all the perturbed quantities, ω is the eigenfrequency of perturbations, which implies that if $\mathrm{Im}(\omega) > 0$ the perturbations grow exponentially and the system is unstable. For the sake of convenience in the subsequent analysis, we introduce the

equation $\Omega = \omega - k_z\beta_{\rm b}c$. Linearizing Eqs. (1) and (2) about the equilibrium state and substituting Eqs. (21) and (22), we obtain the following equations:

$$-\mathrm{i}(\Omega - k_x v_{0x})\delta v_x(y) + \left(\omega_{\rm c} + \frac{\partial v_{0x}}{\partial y}\right)\delta v_y(y) = \mathrm{i}\,k_x\frac{e}{\gamma_{\rm b}m}\delta\psi(y), \tag{24}$$

$$-\omega_{\rm c}\delta v_x(y) - \mathrm{i}(\Omega - k_x v_{0x})\delta v_y(y) = \frac{e}{\gamma_{\rm b}m}\frac{\partial}{\partial y}\delta\psi(y), \tag{25}$$

and

$$-\mathrm{i}(\Omega - k_x v_{0x})\delta n(y) = -\mathrm{i}\,k_x n_0(y)\delta v_x(y) - \frac{\partial}{\partial y}[n_0(y)\delta v_y(y)]. \tag{26}$$

Combining Eqs. (24), (25), and (26), we can derived the general eigenvalue equation as

$$\frac{\partial}{\partial y}\left[\left(1 - \frac{\omega_{\rm p0}^2}{\gamma_{\rm b}^2\xi^2}\right)\frac{\partial}{\partial y}\delta\psi\right] - k_x^2\left(1 - \frac{\omega_{\rm p0}^2}{\gamma_{\rm b}^2\xi^2}\right)\delta\psi = -\frac{k_x\delta\psi}{\Omega - k_x v_{0x}}\frac{\partial}{\partial y}\left(\frac{\omega_{\rm p0}^2\omega_c}{\gamma_{\rm b}^2\xi^2}\right), \tag{27}$$

where $\xi^2 = (\Omega - k_x v_{0x})^2 - \omega_{\rm c}(\omega_{\rm c} + \partial v_{0x}/\partial y)$ and $\omega_{\rm p0}^2 = e^2 n_0/\gamma_{\rm b}m\varepsilon_0$, n_0 is the arbitrary electron density of the equilibrium fluid element.

It is evident that Eq. (27) is a fairly standard second-order eigenvalue problem which can be solved numerically. In order to solve it analytically, we introduce the following assumptions. In addition, it is necessary to make sure that the solutions do not violate the presumptions.

(i) In the case of a sharp boundary and uniform density profile [Eq. (13)], the right-hand side of Eq. (27) becomes a delta function only if

$$\frac{k_x\omega_{\rm p}^2}{\Omega - k_x v_{0x}}\frac{\partial}{\partial y}\left(\frac{\omega_{\rm c}}{\gamma_{\rm b}^2\xi^2}\right) \ll k_x^2\left(1 - \frac{\omega_{\rm p}^2}{\gamma_{\rm b}^2\xi^2}\right). \tag{28}$$

The eigenvalue equation is then simplified to the following form:

$$\frac{\partial}{\partial y}\left[\left(1 - \frac{\omega_{\rm p}^2}{\gamma_{\rm b}^2\xi^2}\right)\frac{\partial}{\partial y}\delta\psi\right] - k_x^2\left(1 - \frac{\omega_{\rm p}^2}{\gamma_{\rm b}^2\xi^2}\right)\delta\psi = -\frac{k_x\omega_{\rm p}^2\omega_{\rm c}\delta\psi}{(\Omega - k_x v_{0x})\,\gamma_{\rm b}^2\xi^2}\left[\delta\left(y + \frac{h}{2}\right) - \delta\left(y - \frac{h}{2}\right)\right], \tag{29}$$

where $\omega_{\rm p}^2 = e^2 n_{\rm b}/\gamma_{\rm b}m\varepsilon_0$.

(ii) Assuming that

$$\frac{\partial}{\partial y}\left(1 - \frac{\omega_{\rm p}^2}{\gamma_{\rm b}^2\xi^2}\right) \ll 1 - \frac{\omega_{\rm p}^2}{\gamma_{\rm b}^2\xi^2}, \tag{30}$$

the piecewise solution for a homogeneous equation can be expressed as

$$\delta\psi(y) = \begin{cases} \dfrac{-\delta\psi(-k_x h/2)[\sinh(k_x y) + \tanh(k_x b/2)\cosh(k_x y)]}{\sinh(k_x h/2) - \tanh(k_x b/2)\cosh(k_x h/2)}, & -b/2 \le y < -h/2, \\ C_1\sinh(k_x y) + C_2\cosh(k_x y), & -h/2 \le y \le h/2, \\ \dfrac{\delta\psi(k_x h/2)[\sinh(k_x y) - \tanh(k_x b/2)\cosh(k_x y)]}{\sinh(k_x h/2) - \tanh(k_x b/2)\cosh(k_x h/2)}, & h/2 < y \le b/2, \end{cases} \tag{31}$$

where the two coefficients C_1 and C_2 are constants. Note that $\omega_{\rm p}^2 = 0$ outside the plasma and there are continuity and jump boundary conditions at the surface of the plasma. Integrating Eq. (29) across the beam-vacuum interfaces at $y = \pm h/2$ and substituting eigenfunction Eq. (31), we can derive the dispersion relation from

$$\begin{vmatrix} a_{11} & a_{12} \\ a_{21} & a_{22} \end{vmatrix} = 0, \tag{32}$$

because C_1 and C_2 do not equal zero simultaneously. Here,

$$a_{11} = \cosh(k_x h/2)(A - k_x hB)\left[(A - k_x hB)^2 - C(C - 2B) - \frac{1}{\gamma_{\rm b}^2}\right] - (A - k_x hB)\left[(A - k_x hB)^2 - C(C - 2B)\right]\sinh(k_x h/2)D - \frac{C\sinh(k_x h/2)}{\gamma_{\rm b}^2}, \tag{33a}$$

$$a_{12} = \sinh(k_x h/2)(A - k_x hB)\left[\frac{1}{\gamma_{\rm b}^2} - (A - k_x hB)^2 + C(C - 2B)\right]$$

$$+(A-k_xhB)\left[(A-k_xhB)^2-C(C-2B)\right]\cosh(k_xh/2)D+\frac{C\cosh(k_xh/2)}{\gamma_{\rm b}^2}, \tag{33b}$$

$$a_{21}=(A+k_xhB)\left[(A+k_xhB)^2-C(C-2B)-\frac{1}{\gamma_{\rm b}^2}\right]\sinh(k_xh/2)D$$
$$-\cosh(k_xh/2)(A+k_xhB)\left[(A+k_xhB)^2-C(C-2B)\right]-\frac{C\sinh(k_xh/2)}{\gamma_{\rm b}^2}, \tag{33c}$$

$$a_{22}=(A+k_xhB)\left[(A+k_xhB)^2-C(C-2B)-\frac{1}{\gamma_{\rm b}^2}\right]\cosh(k_xh/2)D$$
$$-\sinh(k_xh/2)(A+k_xhB)\left[(A+k_xhB)^2-C(C-2B)\right]-\frac{C\cosh(k_xh/2)}{\gamma_{\rm b}^2}, \tag{33d}$$

where we use $\omega_{\rm p}$ to normalize Ω, $\omega_{\rm D}$, and $\omega_{\rm c}$, respectively, for simplicity of notation, and denote those quantities as

$$A=\Omega/\omega_{\rm p}, \tag{34a}$$
$$B=\omega_{\rm D}/\omega_{\rm p}, \tag{34b}$$
$$C=\omega_{\rm c}/\omega_{\rm p}, \tag{34c}$$
$$D=\frac{\cosh(k_xh/2)-\tanh(k_xb/2)\sinh(k_xh/2)}{\sinh(k_xh/2)-\tanh(k_xb/2)\cosh(k_xh/2)}. \tag{34d}$$

For the case of a sheet beam in a strong magnetic field, i.e., $\omega_{\rm c}\gg\omega_{\rm p}$, the general eigenvalue equation (27) can be simplified to

$$\frac{\partial^2}{\partial y^2}\delta\psi-k_x^2\delta\psi=\frac{k_x\delta\psi}{\gamma_{\rm b}^2\omega_{\rm c}\left(\omega-k_xv_{0x}\right)}\frac{\partial\omega_{\rm p}^2}{\partial y}. \tag{35}$$

Likewise, the dispersion relation can be derived from Eq. (32) with a sharp boundary and uniform density profile. As will be seen later, the following equations are also the approximate form of Eq. (33):

$$a_{11}=\frac{-\tanh(k_xb/2)(A-k_xhB)}{\sinh(k_xh/2)-\tanh(k_xb/2)\cosh(k_xh/2)}+2B\sinh(k_xh/2), \tag{36a}$$

$$a_{12}=\frac{A-k_xhB}{\sinh(k_xh/2)-\tanh(k_xb/2)\cosh(k_xh/2)}-2B\cosh(k_xh/2), \tag{36b}$$

$$a_{21}=\frac{\tanh(k_xb/2)(A+k_xhB)}{\sinh(k_xh/2)-\tanh(k_xb/2)\cosh(k_xh/2)}+2B\sinh(k_xh/2), \tag{36c}$$

$$a_{22}=\frac{A+k_xhB}{\sinh(k_xh/2)-\tanh(k_xb/2)\cosh(k_xh/2)}+2B\cosh(k_xh/2), \tag{36d}$$

where A and B are the same as those in the preceding Eqs. (34a) and (34b).

3.2. Comparison between the two cases with and without depending on the restrictive condition $\omega_{\rm c}\gg\omega_{\rm p}$

As we know, the magnetic field may have more difficulty keeping up with the more current carried by the sheet electron beam. The parameter region $\omega_{\rm c}\gg\omega_{\rm p}$ can be broken down easily. For the case of $\omega_{\rm c}\sim\omega_{\rm p}$, it is obvious that the dispersion relation from Eqs. (32) and (36) is not appropriate. Whereas the dispersion relation derived from the general eigenvalue equation is not restricted by the parameter region $\omega_{\rm c}\gg\omega_{\rm p}$, which is just the significant interest of this paper.

In theory, the dispersion relation derived from Eqs. (32) and (36) is a second-order polynomial equation in the form of $(\Omega/\omega_{\rm p})^2=$ constant. The possible solutions of $\Omega/\omega_{\rm p}$ may be a pair of conjugate imaginary numbers or a pair of positive and negative real numbers. As long as the above-mentioned constant on the right-hand side of the equation is negative, the solution of $\mathrm{Im}\,(\Omega/\omega_{\rm p})>0$ will be produced, resulting in growth of perturbations and the instability. Moreover, the dispersion relation determined by Eqs. (32) and (33) is a sixth-order polynomial equation, which can be solved easily to give the eigenfrequency. Furthermore, we need to take notice that the solutions of eigenfrequency should not violate presumptions Eqs. (28) and (30). When $\omega_{\rm c}/\omega_{\rm D}\geq 2$, the minimum requirement for beam confinement is attainable to prevent from being unfocused or trajectory intersect. Hence, the presumptions are satisfied and the solutions are credible in this situation.

According to Eq. (16), the assumption of long axial wavelengths, the diocotron instability occurs in the vicinity of $k_z=0$. If k_z deviates significantly from zero, the instability of shear modes in the z direction appears. In terms of the diocotron instability discussed here, the maximum growth ratio of diocotron instability is identical to the positive imaginary part

of eigenfrequency Ω owing to the relationship $k_z = 0$.

For the purpose of comparison between the two theories with and without the restrictive condition $\omega_c \gg \omega_p$, figure 2 shows the positive imaginary part of normalized eigenfrequency Ω/ω_p versus the ratio ω_c/ω_D of the electron cyclotron frequency to the diocotron frequency, where the same parameters $h = 0.5$ mm, $b = 1.1$ mm, $k_x = 0.1$, and the electron beam voltage $V_0 = 60.2$ kV, the beam current $I_0 = 3.4$ A for the two curves. Here, k_x is a continuous variable and is selected as a small quantity for low-frequency perturbations. The solid line corresponds to the theory depending on $\omega_c \gg \omega_p$ and the circle line corresponds to the theory without depending on $\omega_c \gg \omega_p$. Figure 2 demonstrates that the two curves agree well with each other when the condition $\omega_c \gg \omega_D$ (namely $\omega_c^2 \gg \omega_p^2$) is satisfied. However, the diocotron growth ratio of the case without the restrictive condition $\omega_c \gg \omega_p$ is much larger than the case with the restrictive condition $\omega_c \gg \omega_p$ near ω_c on the order of ω_D. It can be concluded that the preceding diocotron instability analysis with the dispersion relation from Eqs. (32) and (36) can only be applied to the special class of electron beam in the strong magnetic field. Our current investigation with the results Eqs. (32) and (33) certainly have extended the parameter region for focusing magnetic fields.

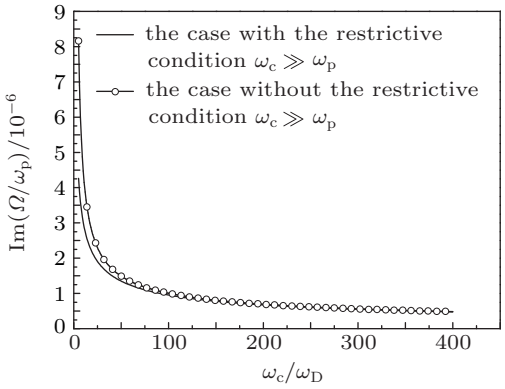


Fig. 2. The positive imaginary part of normalized eigenfrequency Ω/ω_p versus the ratio ω_c/ω_D of the electron cyclotron frequency to the diocotron frequency. The solid line corresponds to the theory with the parameter region $\omega_c \gg \omega_p$ and the circle line corresponds to the theory without the parameter region $\omega_c \gg \omega_p$.

3.3. Diocotron instability properties

For the sheet beam in a strong magnetic field, the diocotron instability is completely stabilized if the conductor gap is less than twice the beam thickness, while the diocotron mode disappears if the conducting walls are brought into contact with the beam. In general, the closer the conducting walls to the beam are, the more stable the diocotron instability is, as expected theoretically and discussed in previous work.[9]

For the sheet beam in a general parameter region of the magnetic field, figure 3 shows the positive imaginary part of normalized eigenfrequency Ω/ω_p versus the ratio h/b of the beam thickness to the conductor gap for various values of ω_c/ω_D. The variation versus ω_c/ω_D is identical with the variation versus ω_c/ω_p from Eq. (15). Figure 3 illustrates that the diocotron instability starts to show at a certain value represented as a threshold λ_b and the diocotron modes do not exist if h/b is larger than this value. Namely, the diocotron perturbations are stabilized with the increase in the ratio h/b. The threshold λ_b decreases to approach 0.5 as the value of ω_c/ω_D increases. The larger the ratio ω_c/ω_D is, the smaller the value of λ_b is, at which the diocotron instability begins. In other words, the smaller the ratio ω_c/ω_D is, the smaller the beam-wall gap needed to ensure the beam stable is. For instance, if $\omega_c/\omega_D = 40$, then it is obvious that $\lambda_b \approx 0.52$. We should design the ratio h/b to be larger than 0.52 or make the ratio of the normalized beam-wall gap to the conductor gap smaller than 0.24 in order to restrain the instability. Likewise, if $\omega_c/\omega_D = 8$, the value of λ_b is identical with about 0.58. As a result, one of the most effective ways to control diocotron instability is to keep the beam-wall gap narrow enough.

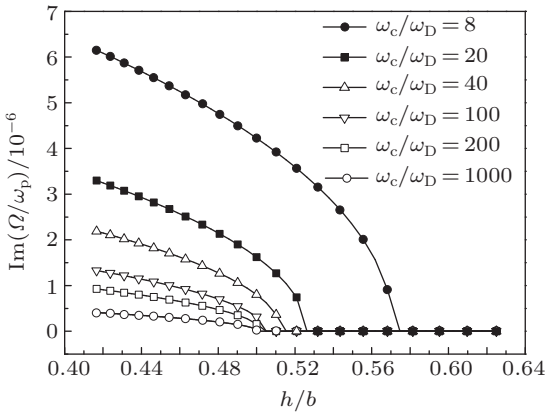


Fig. 3. The positive imaginary part of normalized eigenfrequency Ω/ω_p versus the ratio h/b of the beam thickness to the conductor gap for various values of ω_c/ω_D.

Figure 4 shows the variation of the positive imaginary part of normalized eigenfrequency Ω/ω_p with k_x, in which the structure parameters $h = 0.5$ mm, $b = 1.1$ mm and $\omega_c/\omega_D = 100$. The growth rate of the diocotron instability augments as k_x increases.

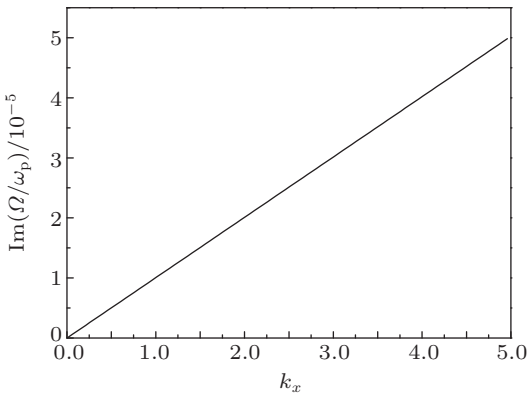


Fig. 4. The variation of the positive imaginary part of normalized eigenfrequency Ω/ω_p with k_x.

Figure 5 shows the variation of the positive imaginary part of normalized eigenfrequency Ω/ω_p with γ_b. The growth rate of the diocotron instability is proportional to the diocotron frequency.[6] The diocotron frequency in Eq. (15) is inversely proportional to γ_b^2, thereby being reduced considerably for a relativistic electron beam. Therefore, the relativistic electron beam is another effective way to suppress the diocotron perturbations.

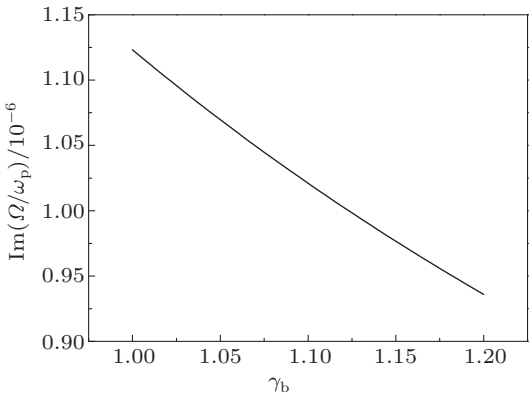


Fig. 5. The variation of the positive imaginary part of normalized eigenfrequency Ω/ω_p with γ_b.

4. Conclusion

The diocotron instability of an infinitely wide relativistic sheet electron beam in grounded conducting walls propagating through a uniform magnetic field is investigated in this paper by making use of the macroscopic cold-fluid model. A more general type of treatment of the diocotron instability has been considered, especially in the case of a higher beam current and a lower magnetic field. The general eigenvalue equation [Eq. (27)] and the dispersion relation [Eqs. (32) and (33)] of the diocotron instability are obtained for low-frequency perturbations with long axial wavelengths. They are very different from the case depending on the restrictive condition of $\omega_\mathrm{c} \gg \omega_\mathrm{p}$, which can only be applied to the special class of a sheet electron beam in a strong magnetic field. Then, we take the parameters of a sheet beam klystron as an example and use the dispersion relation to investigate the diocotron instability for a broad range of system parameters, including the ratio h/b of the beam thickness to the conductor gap, the wave number k_x in the x direction of the perturbations and the relativistic mass factor γ_b. It is found that the growth rate of the diocotron instability is proportional to k_x and inversely proportional to γ_b^2. The transport of a sheet electron beam will be completely stabilized by augmenting the ratio h/b larger than a threshold λ_b, which is dependent on the parameter $\omega_\mathrm{c}/\omega_\mathrm{D}$ greatly. The larger $\omega_\mathrm{c}/\omega_\mathrm{D}$ is, the smaller λ_b will be needed. Therefore, the best way to suppress the diocotron instability is stabilization of the perturbations, either by keeping the beam-wall gap narrow enough according to the numerical calculation in Fig. 3 or by means of the relativistic electron beam. The formula and the way of numerical calculation in the paper can be used commonly to discuss the diocotron instability of a sheet electron beam.

In summary, diocotron instability can be prevented by making use of an appropriate choice of system parameters. It is possible to accomplish the stable transport of a sheet electron beam in axial uniform magnetic field.

References

[1] Webster H F 1955 *J. Appl. Phys.* **26** 1386
[2] Kyhl R L and Webster H F 1956 *IRE Trans. Electron Devices* **ED-3** 172
[3] Cutler C C 1956 *J. Appl. Phys.* **27** 1028
[4] Pierce J R 1956 *IRE Trans. Electron Devices* **ED-3** 183
[5] Buneman O 1957 *J. Electron. Control* **3** 507
[6] Antonsen Jr T M and Ott E 1975 *Phys. Fluids* **18** 1197
[7] Davidson R C 1990 *Physics of Nonneutral Plasmas* (MA: Addison-Wesley) p. 289
[8] Chen H C 1992 *Phys. Fluids* B **4** 1412
[9] Uhm H S, Ben-Menahem S and Yu D 1994 *Phys. Plasmas* **1** 3686
[10] Booske J H, McVey B D and Antonsen Jr T M 1993 *J. Appl. Phys.* **73** 4140
[11] Booske J H, Basten M A, Kumbasar A H, Antonsen Jr T M, Bidwell S W, Carmel Y, Destler W W, Granatstein V L and Radack D J 1994 *Phys. Plasmas* **1** 1714
[12] Burke A, Besong V, Granlund K, Jensen A J, Jongewaard E, Phillips R, Rauenbuehler K, Scheitrum G and Steele R 2006 *Proc. IEEE International Vacuum Electronics Conference* 2006 April 25–27 (IEEE, Monterey) Vol. 1, p. 485
[13] Zhao D 2010 *Acta Phys. Sin.* **59** 1712 (in Chinese)
[14] Ruan C J, Wang S Z, Han Y and Li Q S 2011 *Acta Phys. Sin.* **60** 084105 (in Chinese)